Atomistic Texture of Amorphous Manganese Oxides for Electrochemical Water Splitting Revealed by *Ab Initio* Calculations Combined with X-Ray Spectroscopy

Supporting Information

Giuseppe Mattioli, ∗ , † Ivelina Zaharieva, ‡ Holger Dau, ‡ and Leonardo Guidoni ¶

† Istituto di Struttura della Materia del CNR, v. Salaria Km 29,300 - C.P. 10 I-00015 - Monterotondo Stazione (RM) Italy, ‡ Fachbereich Physik, Freie Universität Berlin, Arnimallee 14, 14195 Berlin, Germany., and ¶ Dipartimento di Scienze Fisiche e Chimiche, Università degli Studi de L'Aquila, Via Vetoio 2, Coppito, I-67100 L'Aquila, Italy

E-mail: giuseppe.mattioli@ism.cnr.it

S1. Additional details of XAS measurements and analyses.

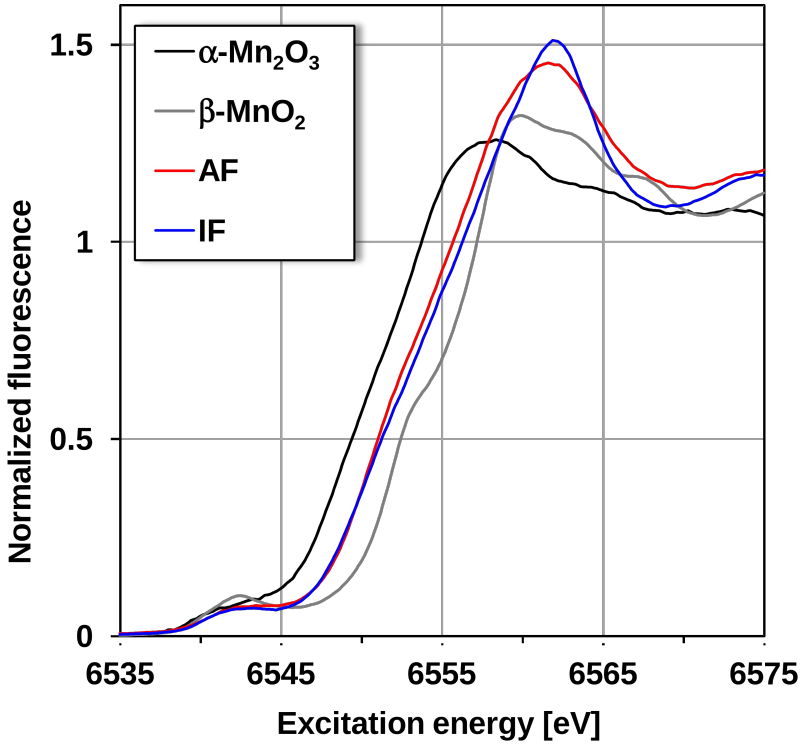

Figure S1. *Mn K-edge XANES spectra of AF, IF, and two reference powders with Mn oxidation state +3.0 and +4.0.*

Table S-I: Simulation parameters for the fit shown in Figure 2 (main text). *Parameters marked by an asterisk (*) were fixed during the least-square fit of the EXAFS spectra, to minimize correlations between fit parameters. For each shell of backscattering atoms, the values in the second row represent the 68% confidence intervals of the respective fit parameters. MS superscript indicates that multiple scattering contributions were included in the simulation.*

Active Film			
Shell	**R [Å]**	**N**	**σ [Å]**
Mn – O	1.89, <0.01	4.6, 0.2	0.061, 0.003
Mn – Mn	2.89, 0.01	5.0, 0.8	0.098, 0.007
Mn – Mn	3.12, 0.01	1.5, 0.3	0.063*
Mn – Mn	3.48, 0.02	0.6, 0.3	0.063*
Mn – Mn	3.79, 0.03	0.6, 0.3	0.063*
Mn – Mn	5.05, 0.03	1.1, 0.6	0.063*
Mn – Mn	5.42, 0.04	1.1, 0.8	0.063*
Mn – Mn^{MS}	2 × 2.89*	0.3, 0.3	0.063*

Inactive Film			
Shell	**R [Å]**	**N**	**σ [Å]**
Mn – O	1.90, <0.01	4.8, 0.4	0.056, 0.005
Mn – Mn	2.88, <0.01	6.7, 1.0	0.074, 0.006

Mn – Mn	3.13, 0.01	1.8, 0.5	0.063*
Mn – Mn	3.53, 0.01	2.3, 0.6	0.063*
Mn – Mn	3.75, 0.05	0.7, 0.7	0.063*
Mn – Mn	5.05, 0.03	2.2, 1.1	0.063*
Mn – Mn	5.55, 0.02	4.6, 1.8	0.063*
Mn – Mn^{MS}	2×2.88*	0.7, 0.7	0.063*

Table S-II: Simulation parameters for the fit shown in Figure 7 (main text). *All the Debye-Waller factors were fixed to the value of 0.039 Å (a value chosen to account only for the relatively low dynamic broadening at 20 K, assuming that each interatomic distance is modelled by a separate shell and thus static broadening is not included). For each shell of backscattering atoms, the values in the second row represent the 68% confidence intervals of the respective fit parameters.*

Active Film

Shell	**R [Å]**	**N**
Mn – O	1.85, 0.01	2.3, 0.2
Mn – O	1.94, 0.01	2.4, 0.2
Mn – O	2.28, 0.01	0.5, 0.1
Mn – Mn	2.83, <0.01	1.8, 0.1
Mn – Mn	2.95, <0.01	2.0, 0.1
Mn – Mn	3.12, <0.01	1.2, 0.1
Mn – Mn	3.49, 0.01	0.4, 0.1
Mn – Mn	3.79, 0.01	0.3, 0.1
Mn – Mn	4.27, 0.03	0.2, 0.1
Mn – Mn	4.89, 0.02	0.8, 0.3
Mn – Mn	5.04, 0.01	1.2, 0.3
Mn – Mn	5.43, 0.01	2.2, 0.3
Mn – Mn	5.58, 0.01	2.4, 0.4

Inactive Film

Shell	**R [Å]**	**N**
Mn – O	1.95, 0.02	2.3, 0.06
Mn – O	1.87, 0.01	2.7, 0.06
Mn – O	2.37, 0.01	1.2, 0.03
Mn – Mn	2.84, 0.01	3.3, 0.03
Mn – Mn	2.95, 0.01	2.3, 0.03
Mn – Mn	3.14, 0.01	1.2, 0.02
Mn – Mn	3.53, 0.01	1.6, 0.02
Mn – Mn	3.71, 0.03	0.4, 0.03
Mn – Mn	4.24, 0.02	0.8, 0.03
Mn – Mn	4.95, 0.01	2.3, 0.06
Mn – Mn	5.08, 0.01	2.9, 0.06
Mn – Mn	5.52, 0.01	4.9, 0.08
Mn – Mn	5.64, 0.01	4.7, 0.08

S2. Pyrolusite MnO_2 and monoclinic $Ca_2Mn_3O_8$ periodic crystals.

The DFT+U(Mn,O) approach discussed in the “Methods” Section of the main text has been

applied to two Mn-oxide crystals whose structure was well-investigated and fully resolved by X-ray diffraction: the pyrolusite MnO_2 (rutile) crystal,[1] and the synthetic $Ca_2Mn_3O_8$.[2]

Table S-III: Pyrolusite MnO_2 (Rutile) lattice parameters and selected interatomic distances.

Method	a	c	Mn-O(a)	Mn-O(b)	Mn-Mn 1	Mn-Mn 2
PBE	4.424	2.874	1.888	1.904	2.874	3.443
U(Mn,O)	4.408	2.920	1.903	1.896	2.920	3.442
Exp XRD	4.396	2.871	1.891	1.877	2.871	3.424

In the case of MnO_2 DFT+U(Mn,O) results are compared with those obtained by using a non-corrected PBE functional. The tetragonal rutile unit cell has been sampled by using a 8x8x8 k-points mesh and the same parameters discussed in the main text. Atomic positions and lattice parameters have been fully optimized without constraint by using the variable-cell BFGS minimization procedure implemented in Quantum-ESPRESSO. Both PBE and DFT+U(Mn,O) approaches provide very good structural results. It may be noted that the elusive distortion of $Mn(IV)O_6$ octahedra, characterized by a Mn-O(a) distance slightly longer than the Mn-O(b) one, is well reproduced only in the case of DFT+U(Mn,O).

Table S-IV: Monoclinic $Ca_2Mn_3O_8$ lattice parameters and selected interatomic distances.

Method	a	b	c	alpha
PBE	11.076	5.887	4.982	109.69
U(Mn,O)	11.042	5.908	4.995	109.84
Exp XRD	11.014	5.851	4.942	109.75

$Ca_2Mn_3O_8$ selected interatomic distances (values in Å, labels in Ref. 2)						
Method	**Mn(1)-O(1)**	**Mn(1)-O(2)**	**Mn(2)-O(1)**	**Mn(2)-O(2)**	**Mn(2)-O(3)**	**Mn(1)-Mn(2)**
PBE	1.913	1.928	1.905	2.016	1.873	2.921
U(Mn,O)	1.910	1.929	1.900	2.000	1.875	2.925
Exp XRD	1.896	1.913	1.891	2.008	1.863	2.899

PBE and DFT+U(Mn,O) calculations have been also performed in the case of $Ca_2Mn_3O_8$. In this case, the monoclinic unit cell has been sampled by using a 4x4x4 k-points mesh. Again, both the approaches provide very good structural results in a layered crystal, which is expected to be more similar to the MnCat structure.

We note that all the Mn-Mn and Mn-O measured distances are reproduced within the limit of a 1% overestimation in both the MnO_2 and $Ca_2Mn_3O_8$ compounds. The DFT+U(Mn,O) approach has to be preferred because it is more suitable to reproduce the correct coupling between oxygen 2p and metal 3d orbitals which characterizes such class of transition metal-oxo compounds (see Ref. 3 and references therein) and, therefore, to simulate in an accurate but cost-effective way both structural and electronic properties of the MnCat.

S3. Complete summary of the structural properties of the investigated Mn_6-Mn_{20} Clusters.

The structural properties of all of the investigated clusters, all sketched as ball-and-stick models in Figures S2-S5, are synthetically summarized in the following Tables S-V-S-X, containing average values and standard deviations of the same Mn-O and Mn-Mn shells discussed in the main text. As opposed to the main text, two different values are reported in the case of the Mn-O first shell. The former (inner) value corresponds to -oxo- bridges only, while the latter (all) value includes also the contributions of terminal Mn-OH and Mn-OH_2 distances but those longer than 2.4 Å (see also Figure 4 in the main text). The shell Mn-Mn 5* does not appear in the A-E models discussed in the main text, but it is detected by EXAFS, as reported in Tables S-I and S-II. It corresponds to the next-neighbor distance involving out-of-plane Mn atoms, as detailed below (see Figure S3, Table S-VI and related text).

Table S-V: A-type clusters.

Model (Mn ox. st.)	**Mn-O (inner)**	**Mn-O (all)**	**Mn-Mn 1**	**Mn-Mn 2/ Mn-Mn 2***	**Mn-Mn 3**	**Mn-Mn 5***	**Mn-Mn 5**
	DFT+U						
A1 (4.00)	1.91 0.06	1.92 0.06	2.88 0.06	-	4.99 0.04	-	5.77 0.01
A1 (3.86)	1.93 0.07	1.94 0.08	2.91 0.08	-	5.04 0.08	-	5.82 0.08
A1 (3.71)	1.95 0.09	1.96 0.10	2.94 0.09	-	5.09 0.12	-	5.88 0.08
A1 (3.57)	1.96 0.10	1.98 0.12	2.97 0.08	-	5.14 0.11	-	5.93 0.02
A2 (4.00)	1.91 0.05	1.92 0.07	2.89 0.05	-	5.02 0.06	-	5.79 0.06
A2 (3.74)	1.94 0.08	1.96 0.10	2.93 0.06	-	5.07 0.07	-	5.85 0.05
A3 (4.00)	1.90 0.06	1.92 0.07	2.89 0.06	-	4.99 0.06	-	5.78 0.06
A4 (4.00)	1.90 0.06	1.92 0.07	2.88 0.06	-	4.98 0.09	-	5.73 0.07
A5 (4.00)	1.92 0.07	1.93 0.10	2.89 0.09	-	4.98 0.08		5.74 0.10
	B3LYP						
A1 (4.00)	1.92 0.07	1.93 0.07	2.90 0.07	-	5.02 0.06	-	5.79 0.05
A1 (3.86)	1.93 0.08	1.94 0.09	2.93 0.09	-	5.07 0.09	-	5.85 0.07
A1 (3.71)	1.95 0.09	1.96 0.10	2.95 0.10	-	5.11 0.06	-	5.91 0.15
A1 (3.57)	1.97 0.11	1.99 0.12	2.99 0.09	-	5.17 0.12	-	5.96 0.02

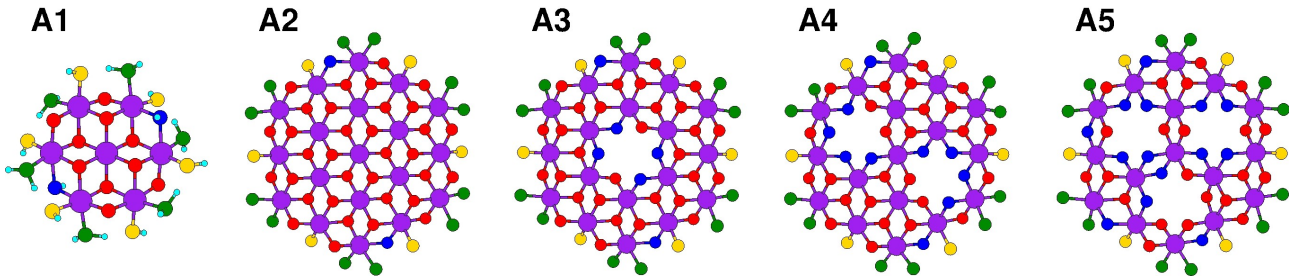

Figure S2. *Ball-and-stick models of the flat A-type clusters*

Negligible structural differences have been found in the larger and defective A2-A5 clusters with respect to the small A1 model discussed in the main text. In the case of the A2 cluster, the starting guess related to the (3.74) average oxidation state of Mn atoms was set in order to localize five Mn(III) sites in a row, by forcing the localization of five excess electrons on five Mn(IV) atoms, distorted to simulate the giant Jahn-Teller effect which characterizes Mn(III) sites. Such Mn(III) sites in a row are not stable. At the end of the geometry optimization the Mn(III) sites are scattered all around the cluster center, always in external Mn sites where the Jahn-Teller distortion is able to involve terminal Mn-OH_2 species (green atoms in Figure S2), as also discussed in the main text.

Table S-VI: B-type clusters.

Model (Mn ox. st.)	**Mn-O (inner)**	**Mn-O (all)**	**Mn-Mn 1**	**Mn-Mn 2/ Mn-Mn 2***	**Mn-Mn 3**	**Mn-Mn 5***	**Mn-Mn 5**
	DFT+U						
B1 (4.00)	1.91 0.07	1.92 0.07	2.86 0.06	3.52 0.04	4.96 0.05	-	5.73 0.01
B1 (3.86)	1.92 0.07	1.94 0.09	2.86 0.06	3.53 0.05	4.96 0.06	-	5.73 0.05
B1 (3.71)	1.93 0.07	1.95 0.09	2.89 0.08	3.53 0.07	5.00 0.11	-	5.77 0.14
B1 (3.57)	1.95 0.09	1.95 0.09	2.93 0.10	3.51 0.08	5.07 0.14	-	5.85 0.17
B2 (4.00)	1.91 0.06	1.92 0.07	2.89 0.06	3.51 0.04	4.97 0.06	5.41 0.05	5.75 0.06
B3 (4.00)	1.91 0.06	1.92 0.07	2.87 0.06	3.51 0.07	4.96 0.08	5.37 0.06	5.70 0.07
B3 (3.94)	1.91 0.06	1.93 0.08	2.89 0.06	3.52 0.02	4.97 0.06	5.42 0.02	5.76 0.06
B3 (3.89)	1.92 0.07	1.94 0.10	2.89 0.06	3.50 0.05	4.99 0.06	5.38 0.08	5.78 0.12
B3 (3.79)	1.93 0.09	1.96 0.11	2.91 0.07	3.50 0.05	5.01 0.07	5.37 0.10	5.83 0.12
	B3LYP						
B1 (4.00)	1.92 0.08	1.92 0.08	2.88 0.08	3.55 0.06	4.98 0.06	-	5.75 0.01

B1 (3.86)	1.92 0.09	1.94 0.11	2.87 0.08	3.57 0.07	4.97 0.06	-	5.74 0.04
B1 (3.71)	1.93 0.10	1.95 0.10	2.88 0.09	3.58 0.10	4.99 0.14	-	5.76 0.19
B1 (3.57)	1.94 0.08	1.95 0.09	2.92 0.09	3.52 0.10	5.05 0.13		5.83 0.15

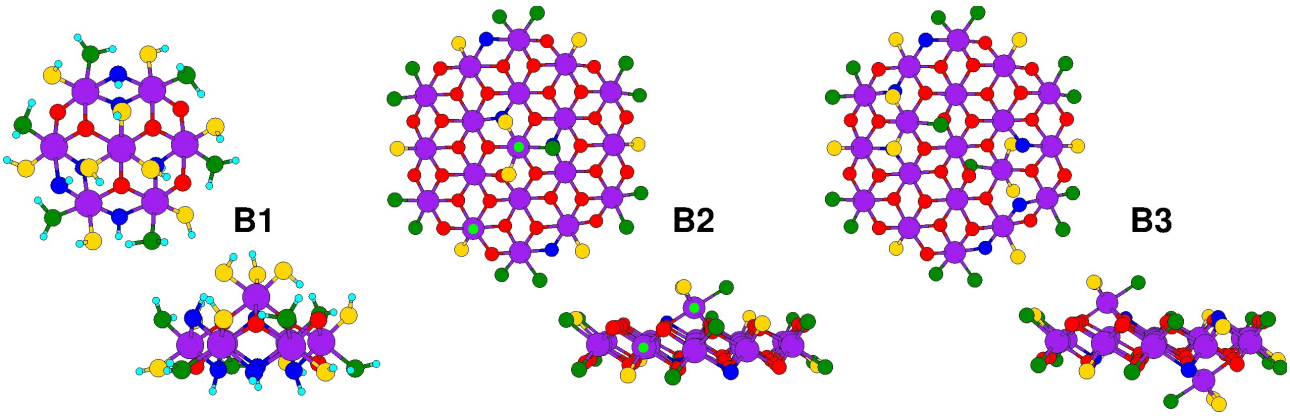

Figure S3. *Ball-and-stick models of the B-type clusters containing out-of-plane Mn atoms. The light-green dots in the B2 cluster exemplify the Mn-Mn 5* subshell.*

As opposed to the A-type clusters, the Mn-Mn 5* distance measured by EXAFS is present in the B-type clusters and assigned to the next-neighbors of out of plane Mn atoms (see the light-green dots in Figure S3).

Table S-VII: C-type clusters.

Model (Mn ox. st.)	**Mn-O (inner)**	**Mn-O (all)**	**Mn-Mn 1**	**Mn-Mn 2/ Mn-Mn 2***	**Mn-Mn 3**	**Mn-Mn 5***	**Mn-Mn 5**
	DFT+U						
C1 (4.00)	1.93 0.07	1.94 0.09	2.93 0.07	4.20 0.19	5.05 0.13	-	5.86 0.11
C1 (3.75)	1.94 0.08	1.95 0.10	2.95 0.08	4.19 0.22	5.08 0.13	-	5.89 0.12
C1 (3.50)	1.98 0.12	1.99 0.13	2.99 0.08	4.14 0.09	5.15 0.12	-	5.99 0.08
	B3LYP						
C1 (4.00)	1.94 0.10	1.95 0.11	2.94 0.07	4.20 0.17	5.06 0.13	-	5.87 0.12
C1 (3.75)	1.95 0.11	1.96 0.12	2.96 0.09	4.17 0.20	5.09 0.14	-	5.91 0.13
C1 (3.50)	1.98 0.11	1.98 0.12	2.98 0.08	4.19 0.13	5.15 0.12	-	5.98 0.02

The only investigated C-type cluster, having an out-of-plane Mn atom which close a complete cubane-like unit, is shown in Figure 3 of the main text. We note that in this case the next-

neighbors of the out of plane Mn atom are found at about 5 Å, and fall therefore within the in-plane Mn-Mn 3 shell.

Table S-VIII: D-type clusters.

Model (Mn ox. st.)	Mn-O (inner)	Mn-O (all)	Mn-Mn 1	Mn-Mn 2/ Mn-Mn 2*	Mn-Mn 3	Mn-Mn 5*	Mn-Mn 5
	DFT+U						
D1 (4.00)	1.92 0.06	1.92 0.07	2.90 0.07	3.48 0.04	4.93 0.19	-	5.81 0.14
D1 (3.90)	1.92 0.07	1.93 0.07	2.92 0.11	3.50 0.05	5.01 0.19	-	6.07 0.29
D1 (3.80)	1.94 0.11	1.95 0.10	2.93 0.11	3.52 0.07	5.02 0.17	-	6.06 0.32
D1 (3.60)	1.96 0.11	1.97 0.12	2.96 0.11	3.52 0.11	5.00 0.20		6.05 0.28
D2 (4.00)	1.93 0.03	1.91 0.05	2.90 0.01	-	5.00 0.03	-	5.79 0.01
D3 (4.00)	1.94 0.04	1.91 0.06	2.92 0.05	-	5.02 0.13	-	5.83 0.02
D3 (3.83)	1.96 0.09	1.94 0.10	2.95 0.07	-	5.06 0.18	-	5.79 0.04
D3 (3.67)	1.97 0.11	1.96 0.11	2.96 0.06	-	5.08 0.04	-	5.88 0.03

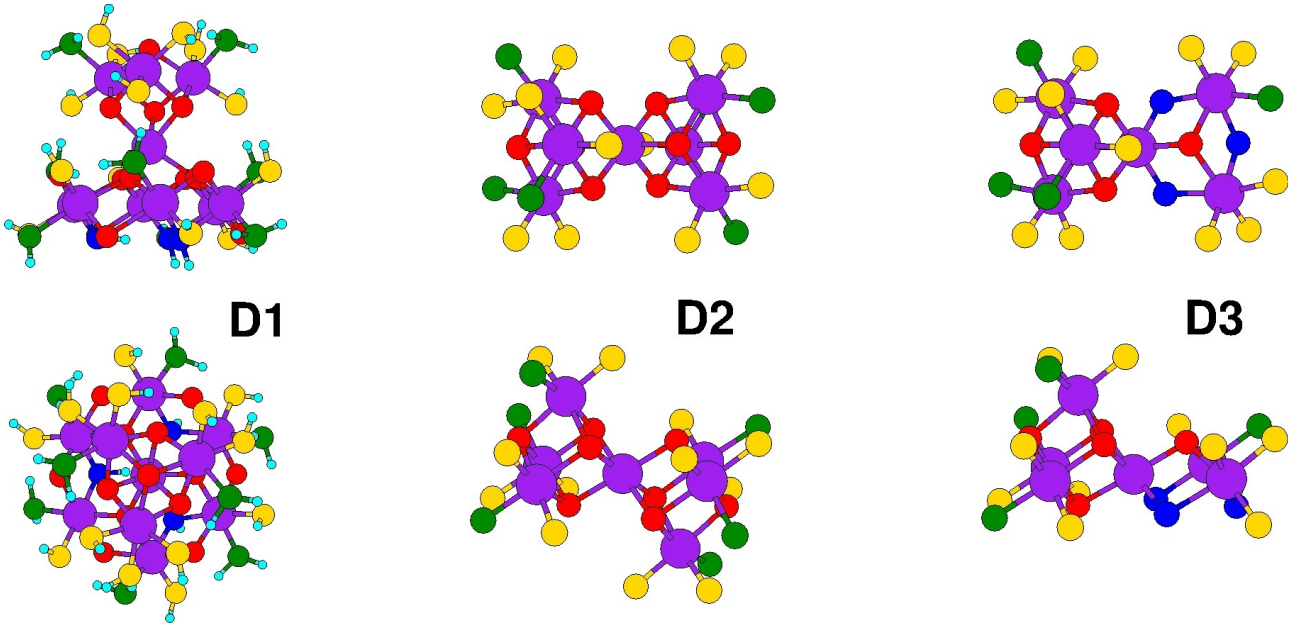

Figure S4. *Ball-and-stick models of the D-type clusters containing one or more closed cubane-like units not contained in the Mn-oxo sheet.*

All the investigated closed cubane-like units contained in the C-type and D-type clusters are characterized by Mn-Mn 1 distances slightly longer than those reported in the case of open structures, as discussed in detail in the main text.

Table S-IX: E-type clusters.

Model (Mn ox. st.)	Mn-O (inner)	Mn-O (all)	Mn-Mn 1	Mn-Mn 2/ Mn-Mn 2*	Mn-Mn 3	Mn-Mn 5*	Mn-Mn 5
	DFT+U						
E1 (3.85)	1.93 0.10	1.94 0.10	2.86 0.06	3.65 0.05	4.89 0.17	-	5.75 0.07
E1 (3.69)	1.94 0.11	1.96 0.11	2.88 0.07	3.66 0.08	4.89 0.17		5.79 0.13
E1 (3.54)	1.97 0.13	1.98 0.13	2.91 0.08	3.70 0.13	4.93 0.19		5.82 0.17

The only investigated E-type cluster, having an out-of-plane Mn(II) atom shared between two Mn-oxo sheets, is shown in Figure 3 of the main text.

Table S-X: F-type clusters.

Model (Mn ox. st.)	Mn-O (inner)	Mn-O (all)	Mn-Mn 1	Mn-Mn 2/ Mn-Mn 2*		Mn-Mn 3	Mn-Mn 5*	Mn-Mn 5
	DFT+U							
F1 (4.00)	1.93 0.05	1.92 0.07	2.95 0.10	3.49 0.04	4.52 0.08	5.00 0.10	5.41 0.09	5.80 0.06
F1 (3.80)	1.96 0.10	1.96 0.11	2.96 0.08	3.52 0.08	4.45 0.17	5.06 0.11	5.48 0.05	5.77 0.10
F1 (3.60)	1.96 0.10	1.97 0.12	2.97 0.09	3.54 0.08	4.45 0.16	5.03 0.09	5.35 0.08	5.77 0.13

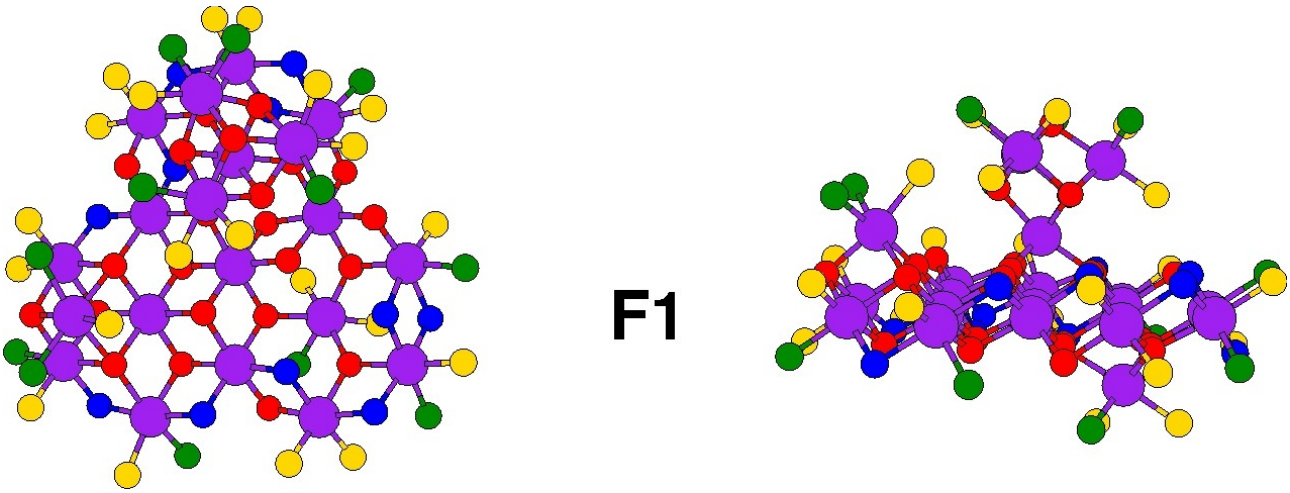

Figure S5. *Ball-and-stick models of the F-type cluster*

The F1 cluster can be considered as a tentative model of a larger structure containing all the motifs which characterize the A-D clusters. All kinds of Mn-O and Mn-Mn distance are therefore represented in Table S-X and their values are reassuringly similar to those calculated in the case of smaller clusters.

S4. Periodic Mn-oxo Sheets.

A small part of the investigation has been devoted to periodic models of the MnCat. The calculations are very demanding because the error on the stress tensor (needed to relax the xy plane of the sheet) is one order of magnitude higher than the error on forces, when calculated on the same ground-state wavefunctions. Hence the periodic calculations require very strict convergence criteria, also including an accurate sampling of the Brillouin Zone (BZ), while the non periodic calculations can be intrinsically performed by using the Γ point only to sample the BZ. We used a periodically repeated Mn_4O_8 sheet, replicated in a 2x2 supercell (a $Mn_{16}O_{32}$ sheet). The BZ has been sampled by a 3x3x1 regular mesh of k-points. Simple defects of the sheet like a Mn vacancy or an "on top" Mn atom have been considered, in close comparison with the previous non-periodic calculations. Defected model are H-saturated, as shown in Figure S6, in order to enforce the correct oxidation state on Mn atoms. The long range order of the sheets induce Mn-Mn distances slightly longer than those calculated in the case of isolated models containing Mn(IV) only.

Table S-XI: Periodic Mn(IV)-oxo models.

	Mn-O (inner)	Mn-O (all)	Mn-Mn 1	Mn-Mn 2	Mn-Mn 3	Mn-Mn 4	Mn-Mn 5
A2-PBC[a]	1.918 1.917	-[b] -[b]	2.921 2.918	- -	5.055 5.060	- -	5.836 5.841
A3-PBC	1.92 0.03	-[b]	2.92 0.03	-	5.05 0.02	-	5.81 0.02
B2-PBC	1.92 0.03	1.92 0.04	2.91 0.02	3.56 0.01	5.04 0.02	5.44 0.01	5.80 0.02

[a] The perfect A2-PBC sheet is characterized by a tiny distortion of the Mn(IV)O_6 octahedra, leading to two different Mn-O and Mn-Mn distances, both reported in the Table. The former distance involves 2/6 of the bonds, the latter distance 4/6.

[b] All the O atoms are inner μ_2-O and μ_3-O bridges.

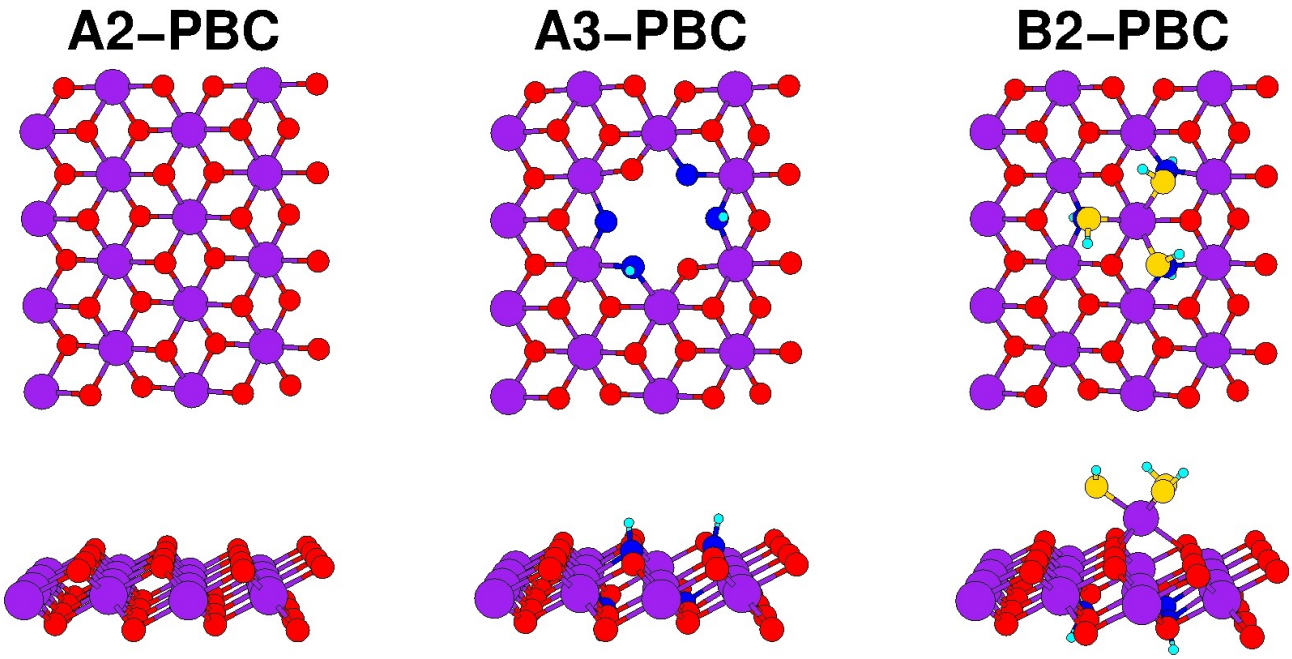

Figure S6. *Ball-and-stick models of regular and defective periodic sheets.*

S5. Magnetic coupling of Mn centers.

Accurate estimates of the magnetic coupling between Mn centers represent an elusive issue for ab initio calculations. The results in terms of ferromagnetic, ferrimagnetic (in the case of Mn(III)-Mn(IV) interactions), and antiferromagnetic ordering are very strongly dependent on the fine tuning of the level of theory employed in the calculation. Conventional DFT-GGA calculations (not employed in the present investigation) generally overestimate the electronic repulsion ("delocalization error"), especially in the case of highly localized d electrons of transition metals. It is well known that the insertion of a given amount of Hartree-Fock exact exchange in a conventional local (LDA) or semilocal (GGA, e.g., PBE) density functional has two competing and well acknowledged effects:[4-6] an effective correction of delocalization error, due to the opposite curvature of Hartree-Fock and LDA (GGA). A worsening (with respect to LDA or GGA) in the description of strongly localized and nearly degenerate electronic states like those which characterize narrow bands arising from transition metals in solids. This effect, known as "static correlation error", is often well understood in terms of a fractional-spin problem: when we pull apart the protons of an H_2 molecule the static correlation error energetically favors configurations in which the electron pair is delocalized on both nuclei (half spin-up and half spin-down). This happens because of the lacking of a derivative discontinuity in exact-exchange (e.g., B3LYP) functionals.[5,6] Such a derivative discontinuity is instead inserted in the DFT+U framework, as clearly explained in all the publications which discuss in detail the rotationally-invariant DFT+U method used to perform the present calculations.[7-9] Magnetic properties calculated at a well-tuned DFT+U level should be therefore considered, *coeteris paribus*, as more reliable.[10,11]

Two series of calculations have been performed, related to the A1 (4.00) and B1 (4.00) cluster discussed above. The results are summarized in Table S-XII. First of all, every single Mn atom is always more stable in a high-spin state, irrespective of the level of theory used. Global low-spin configurations are characterized by structural instabilities and very high energies. In both cases the HS, or ferromagnetic, solution (all the Mn(IV) atoms having 3 unpaired spin-up electrons) has been therefore compared with a BS, or ferrimagnetic, configuration where the spin state of the central Mn atom (in the plane in A1, on top in B1) is flipped. We note that the central atom acts as a "magnetic anchoring point":[12] when its spin is flipped, six ferromagnetically coupled Mn-Mn pairs shift to antiferromagnetic, with potentially high impact on total energies and structures. As expected, BS configurations prevail in the case of B3LYP, even if the difference is very small in the case of the B1 (4.00) cluster. On the contrary, HS configurations are favored in the case of DFT+U for both clusters. Anyway, we can observe that: (a) the energy differences are quite small: we can expect that the magnetic coupling, probably detectable at low temperature, does not affect room temperature catalysis; (b) the magnetic coupling surely does not affect the structural properties of the investigated models: there are practically no structural differences between the investigated high-spin and broken-symmetry structures.

Table S-XII: *Mn-O and Mn-Mn distances and relative energy differences calculated for high-spin (HS) and broken-symmetry (BS) configurations of the A1 and B1 clusters discussed above.*

	Mn-O (inner)	**Mn-O (all)**	**Mn-Mn 1**	**Mn-Mn 2**	**Mn-Mn 3**	**Mn-Mn 5**	**Relative Energy (eV)**
	DFT+U						
A1 (4.00) HS	1.91 0.06	1.92 0.06	2.88 0.06		4.99 0.04	5.77 0.01	0

A1 (4.00) BS	1.91 0.06	1.92 0.06	2.88 0.05		4.98 0.04	5.76 0.01	+0.08
B1 (4.00) HS	1.91 0.07	1.92 0.07	2.86 0.06	3.52 0.04	4.96 0.05	5.73 0.01	0
B1 (4.00) BS	1.91 0.07	1.92 0.07	2.86 0.07	3.52 0.04	4.95 0.05	5.72 0.01	+0.06
	B3LYP						
A1 (4.00) HS	1.92 0.07	1.93 0.07	2.90 0.07		5.02 0.06	5.79 0.05	+0.19
A1 (4.00) BS	1.91 0.06	1.93 0.07	2.90 0.08		5.02 0.06	5.80 0.05	0
B1 (4.00) HS	1.92 0.08	1.92 0.08	2.88 0.08	3.55 0.06	4.98 0.06	5.75 0.01	+0.01
B1 (4.00) BS	1.92 0.08	1.92 0.08	2.88 0.08	3.55 0.06	4.98 0.06	5.75 0.01	0

S6. Bader and Lowdin charge analysis of the E1 (3.69) cluster.

Table S-XIII: *Bader and Lowdin charge analysis of Mn atoms belonging to the E1 (3.69) cluster. The Mn(II) and Mn(III) atoms are contained in yellow and green rows, respectively. Values in the table refer to the Mn valence charge only. 10 further core electrons are embedded into the PAW pseudopotentials. Relative values of total charge are reported in parentheses alongside absolute values.*

Mn atom	UP charge	DOWN charge	TOTAL charge	Polarization
1 Bader	8.34	4.66	12.99 (+2.01)	3.68
1 Lowdin	8.38	4.94	13.32(+1.68)	3.43
2 Bader	8.25	4.70	12.95(+2.05)	3.55
2 Lowdin	8.30	4.99	13.29(+1.71)	3.30
3 Bader	8.25	4.71	12.97(+2.03)	3.54
3 Lowdin	8.29	5.00	13.28(+1.72)	3.29
4 Bader	8.62	4.46	13.08(+1.92)	4.16 - Mn(III)
4 Lowdin	8.63	4.70	13.34(+1.66)	3.93 - Mn(III)
5 Bader	8.27	4.68	12.95(+2.05)	3.59
5 Lowdin	8.32	4.97,	13.29(+1.71)	3.35
6 Bader	8.27	4.72	12.99(+2.01)	3.54
6 Lowdin	8.30	5.01	13.31(+1.69)	3.29
7 Bader	8.99	4.24	13.22(+1.78)	4.75 - Mn(II)
7 Lowdin	8.98	4.43	13.41(+1.59)	4.55 - Mn(II)
8 Bader	8.25	4.72	12.96(+2.04)	3.53
8 Lowdin	8.29	5.01	13.31(+1.69)	3.28

9 Bader	8.23	4.73	12.95(+2.05)	3.50
9 Lowdin	8.28	5.02	13.30(+1.70)	3.26
10 Bader	8.26	4.72	12.98(+2.02)	3.54
10 Lowdin	8.30	5.02	13.32(+1.68)	3.28
11 Bader	8.72	4.49	13.21(+1.79)	4.23 - Mn(III)
11 Lowdin	8.70	4.71	13.41(+1.59)	3.99 - Mn(III)
12 Bader	8.31	4.69	13.00(+2.00)	3.62
12 Lowdin	8.35	4.97	13.32(+1.68)	3.37
13 Bader	8.20	4.74	12.94(+2.06)	3.46
13 Lowdin	8.26	5.04	13.30(+1.70)	3.21

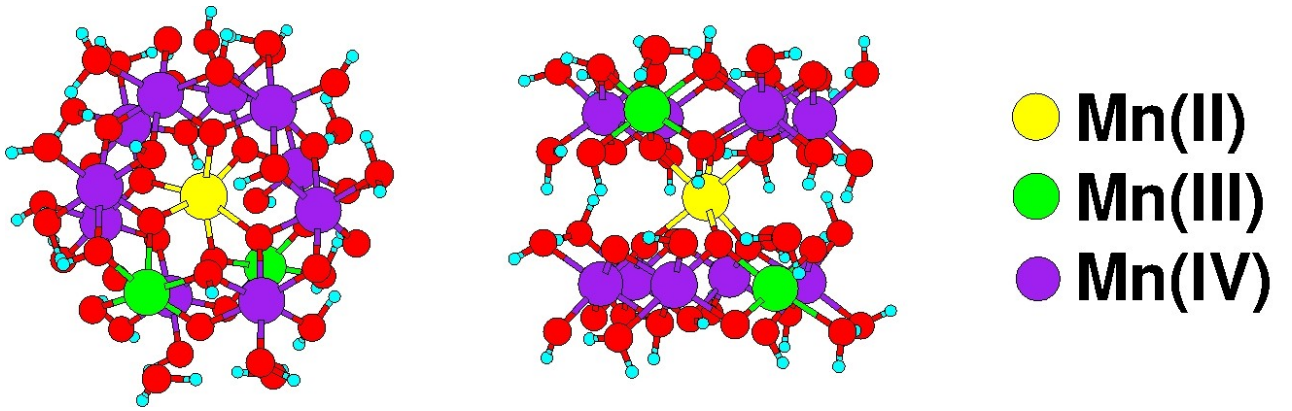

Figure S7. *Ball-and-stick model of the E1 (3.69) cluster.*

The charge distribution between Mn atoms in the E1 (3.69) cluster has been calculated by using the popular Lowdin partitioning scheme and the Bader partitioning scheme,[13-15] based purely on the inherent charge-density distribution of the system. The results are reported in Table S-XIII. As pointed out by Raebiger et al.,[16] transition metal (TM) atoms hosted in insulating or semiconducting compounds are characterized by self-regulation mechanisms that redistribute the charge. As opposed to a more traditional charge-transfer paradigm, where changes in the oxidation states of TM atoms are often tacitly associated with a literal transfer of charge to or from the atoms, recent ab-initio calculations based on unbiased charge-partitioning schemes have been able to show that only negligible changes in the local TM charge can be expected as the oxidation state is altered. We found indeed a full confirmation of such significant success of first-principle theoretical methods in the case of the present analysis. The E1 (3.69) neutral cluster contains four excess electrons with respect to a full distribution of Mn(IV) sites. As detailed in the main text, two electrons are nominally attributed to the Mn(II) atom between the sheets (yellow ball in Figure S7), and two further electrons are nominally attributed to two Mn(III) atoms (green balls in Figure S7). These assignments are basically supported by the structural properties of the Mn(II) center (all six Mn-O bond longer than in $Mn(IV)O_6$, slight angular distortion of the $Mn(II)O_6$ octahedron driven by the interlayer H-bonds only) and of the two Mn(III) centers (giant Jahn-Teller distortion of the d5 $Mn(III)O_6$ octahedra, specially involving terminal $Mn\text{-}OH_2$ species). However, the small differences between total charges discussed above, even if indicative of correct trends and in agreement with structural data, do not represent a solid ground on which quantitative discrimination between Mn sites can be assessed. As an example, Mn(II) (atom 7) and one of the Mn(III) (atom 11) have practically the same Bader and Lowdin charges.

Our results show also that, as opposed to the total charge, the spin polarization of TM atoms, that is, the magnetic properties of Mn centers, can be considered as a more sensitive tool, able to discriminate in a safer and quantitative way the electronic properties of different sites. This is in a good agreement with the fact that electron paramagnetic resonance (EPR) measurements are traditionally employed to investigate the oxidation state of paramagnetic TM atoms in inorganic as well as metallo-organic or biological systems. Large differences between the spin polarization of Mn(II), Mn(III) and Mn(IV) sites, accompanied by values in a closer agreement with the conventional picture of such sites as d5, d4 and d3 configurations, respectively, offer a sound tool to the analysis of the electronic properties of Mn oxides, and confirm the simultaneous occurrence of three different oxidation states of Mn in MnCat.

Finally, we note that even if there are relevant quantitative differences between the ab initio Bader approach and the partially arbitrary Lowdin approach, the latter one provides a correct qualitative discrimination between Mn sites, in close agreement with the more accurate results attributed to the former ones. As Lowdin charges are obtained by using routinary post-processing tools, contained in almost all the ab initio codes, we can reassuringly base the comparison between present and future results on such kind of charge analysis.

References

(1) Wyckoff, R. W. G. *Crystal Structures*; Interscience Publishers, New York, **1963**.

(2) Ansell, G. B.; Modrick, M. A.; Longo, J. M.; Poeppelmeyer, K. R.; Horowitz, H. S.; *Acta Cryst.* **1982**, *B38*, 1795.

(3) Mattioli, G.; Giannozzi, P.; Amore Bonapasta, A.; Guidoni, L. *J. Am. Chem. Soc.* **2013**, *135*, 15353-15363.

(4) Cohen, A. J.; Mori-Sànchez, P.; Yang, W. *Science* **2008**, *321*, 792-794.

(5) Mori-Sànchez, P.; Cohen, A. J.; Yang, W. *Phys. Rev. Lett.* **2009**, *102*, 066403.

(6) Mori-Sànchez, P.; Cohen, A. J. *Phys. Chem. Chem. Phys.* **2014**, *16*, 14378-14386.

(7) Cococcioni, M.; de Gironcoli, S. *Phys. Rev. B* **2005**, *71*, 035105.

(8) Campo Jr., V. L.; Cococcioni, M. *J. Phys.: Condens. Matter* **2009**, *22*, 055602.

(9) Himmetoglu, B.; Floris, A.; de Gironcoli, S.; Cococcioni, M. *Int. J. Quantum Chem*. **2014**, *114*, 14-49.

(10) Scherlis, D. A.; Cococcioni, M.; Sit, P.; Marzari, N. J. Phys. Chem. B **2007**, *111*, 7384.

(11) Cao, C.; Hill, S.; Cheng, H.-P. Phys. Rev. Lett. **2008**, *100*, 167206.

(12) Filippone, F.; Mattioli, G.; Alippi, P.; Amore Bonapasta, A. *Phys. Rev. Lett.* **2011**, 107, 196401.

(13) Tang, W.; Sanville, E.; Henkelman, G. *J. Phys.: Condens. Matter* **2009**, *21*, 084204.

(14) Sanville, E.; Kenny, S. D.; Smith, R.; Henkelman G. *J. Comp. Chem.* **2007**, *28*, 899-908.

(15) Henkelman, G.; Arnaldsson, A.; Jónsson, H. *Comput. Mater. Sci.* **2006**, *36*, 254-360.

(16) Raebiger, H.; Lany, S.; Zunger, A. *Nature* **2008**, *453*, 763-766.